

Supporting information for

Size-Controlled Nanocrystals Reveal Spatial Dependence and Severity of Nanoparticle Coalescence and Ostwald Ripening in Sintering Phenomena

Authors: Emmett D. Goodman¹, Evan Z. Carlson¹, Elisabeth M. Dietze², Nadia Tahsini¹, Arun Johnson¹, Aisulu Aitbekova¹, Temy Nguyen Taylor¹, Philipp Plessow², Matteo Cargnello^{1*}

¹Department of Chemical Engineering and SUNCAT Center for Interface Science and Catalysis, Stanford University, Stanford CA, 94305, USA.

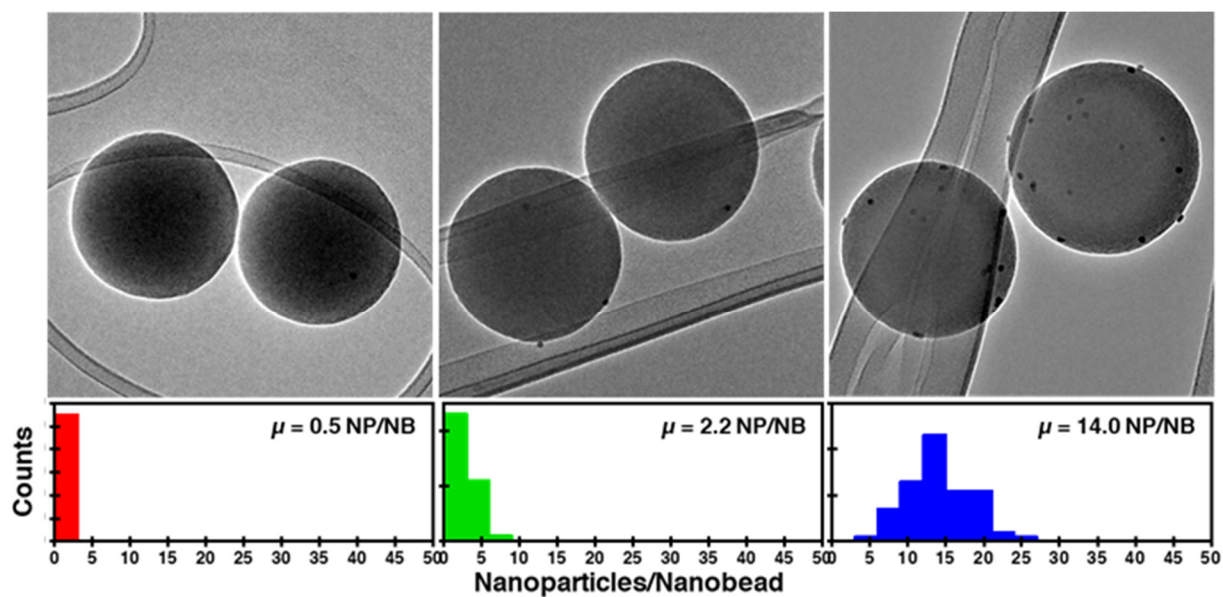
²Institute of Catalysis Research and Technology, Karlsruhe Institute of Technology, Hermann-von-Helmholtz-Platz 1, D-76344 Eggenstein-Leopoldshafen, Germany.

*Correspondence to: mcargn@stanford.edu.

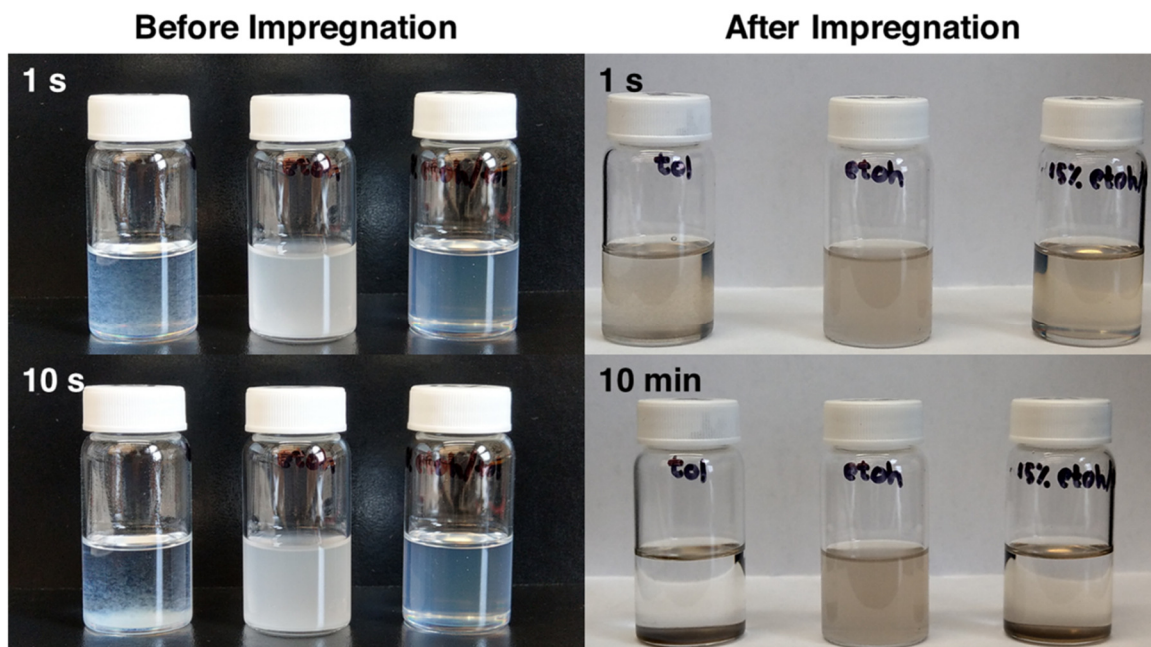
Content:

- Fig. S1: getting NCs to stick: impregnation and support surface chemistry
- Fig. S2: getting NCs to distribute using solvent
- Fig. S3: quantifying impregnation strategies
- Fig. S4: tomography of 8.8 nm Pd/SiO₂ composite
- Fig. S5: density controlled 8.8 nm Pd/SiO₂ composites
- Fig. S6: nearest neighbor distances of simulated Pd NPs on SiO₂ spheres
- Fig. S7: Monte Carlo simulations of coalescence distances
- Fig. S8: ATR-FTIR spectra of 8.8 nm Pd/SiO₂ nanocomposite after aging treatments
- Fig. S9: oxidation state analysis of high-temperature sintering process
- Fig. S10: temperature-programmed O₂ evolution versus nanomaterial stability
- Fig. S11: representative TEM images of 14.7 nm Pd/SiO₂ after various aging treatments
- Fig. S12: particle size area analysis reveals ostwald (atomic) ripening
- Fig. S13: stability study of Pd/SiO₂ synthesized with commercial Davisil SiO₂
- Fig. S14: x-ray photoelectron spectroscopy survey scans of 62-Pd/SiO₂ as-synthesized and after aging.
- Fig. S15: tracking empty SiO₂ spheres on density-controlled 8.8 nm Pd/SiO₂ samples
- Fig. S16: size-dependent vapor phase sintering simulations of metallic Pd
- Fig. S17: rate of atomic emission from surface of 8.8 nm Pd NCs
- Fig. S18: particle size distributions of Au/SiO₂ before and after aging at 800 °C.
- Fig. S19: x-ray photoelectron spectroscopy of 62-Pd/SiO₂ material after aging treatments
- Fig. S20: thermogravimetric analysis of reference PdO materials
-
- Table S1: additional characterization of Pd/SiO₂ materials used in this work
- Table S2: calculations for oxidative expansion of NCs from Pd to PdO
- Table S3: employed experimental data for Ostwald ripening mean-field model

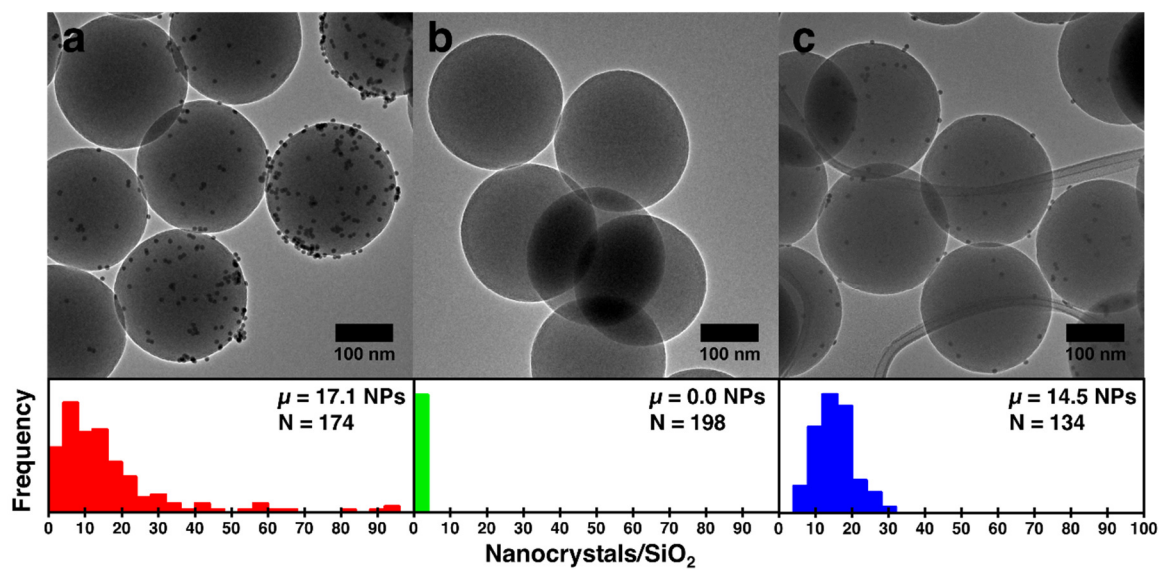
Supporting Figure S1: getting NCs to stick: Pd adhesion to the SiO₂ support is a strong function of the SiO₂ surface chemistry. (Left) calcined SiO₂ spheres, (middle) SiO₂ spheres dried at 75 °C and (right) solvent exchanged SiO₂ spheres. In these experiments, all impregnations were done in toluene.



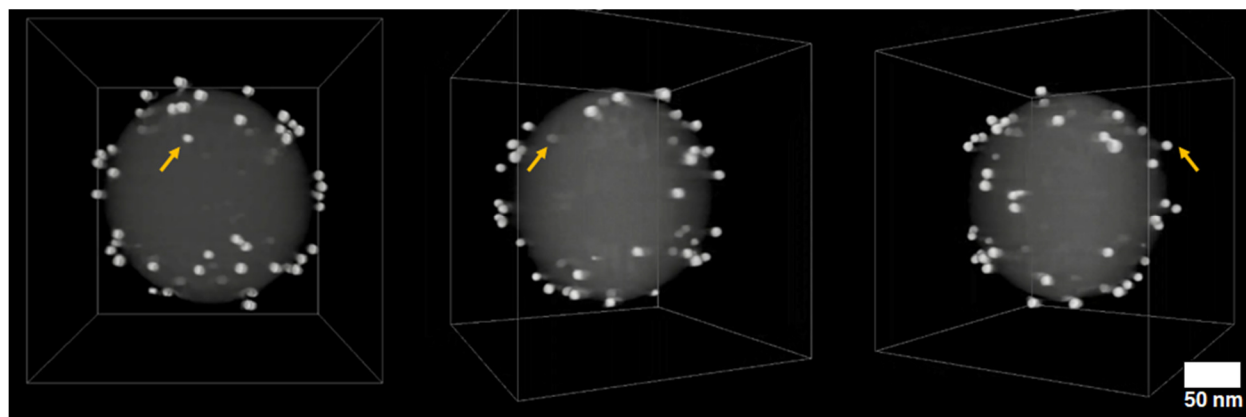
Supporting Figure S2: getting NCs to distribute using solvent. Images of SiO₂ spheres dispersed in different solvents before and after NC impregnation. In each image: toluene (left), ethanol (middle), 15 vol. % ethanol/toluene(right). The addition of small amounts of ethanol to toluene allows for SiO₂ dispersibility, while maintaining the driving force for Pd adhesion.



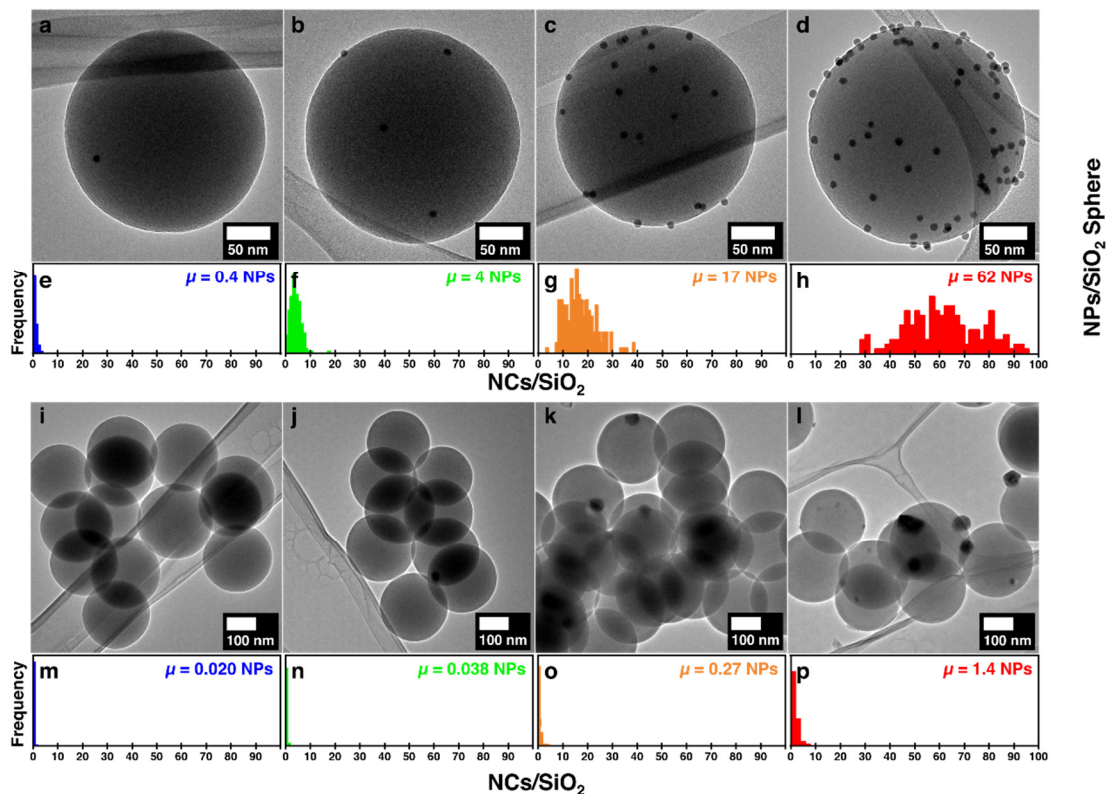
Supporting Figure S3: quantifying impregnation strategies and the effect of impregnation solvent: TEM images (top) and NC/sphere frequency plots (below) of impregnations in (A) toluene, (B) ethanol, and (C) 1:6 vol. ratio ethanol : toluene.



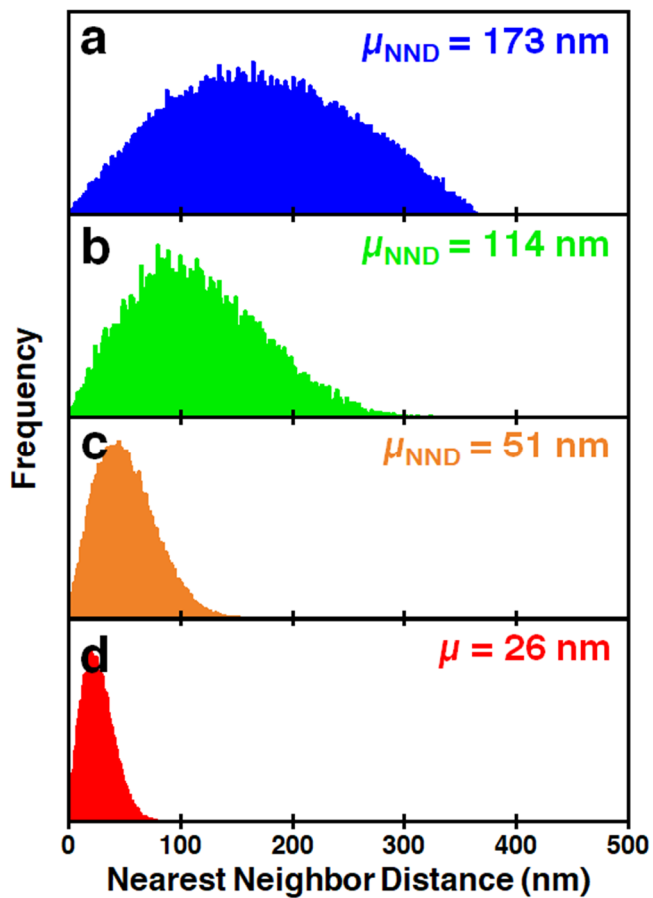
Supporting Figure S4: tomography of 8.8 nm Pd/SiO₂ nanocomposite used in work. Tomography is used to confirm random 3D spatial distribution of Pd NCs on the silica surface. One particle is tracked (yellow arrow) across a 360° rotation.



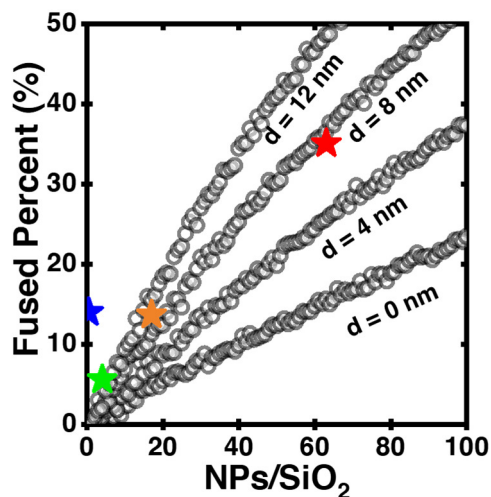
Supporting Figure S5: Representative TEM image and density statistics of 8.8 nm Pd/SiO₂ materials with mean NC-Pd/SiO₂ values of (a,e) 0.3-Pd/SiO₂ (b,f) 4.0-Pd/SiO₂ (c,g) 17-Pd/SiO₂ and (d,h) 62-Pd/SiO₂. After aging at 900 °C for 5 h in static air, representative TEM image and density statistics of (i,m) 0.3-Pd/SiO₂ (j,n) 4.0-Pd/SiO₂ (k,o) 17-Pd/SiO₂ and (l,p) 62-Pd/SiO₂.



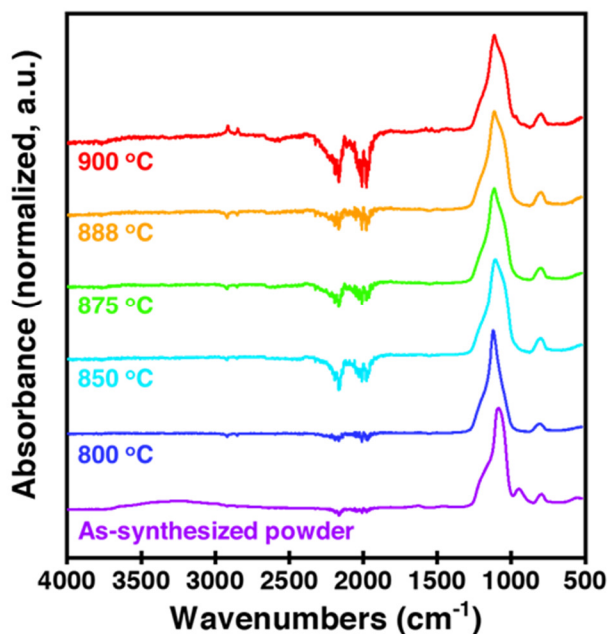
Supporting Figure S6: Nearest neighbor distances of simulated Pd NPs on SiO₂ spheres. Histogram of nearest neighbor distances of ensembles of (a) 0.4 NPs (b) 4 NPs (c) 17 NPs and (d) 62 NPs. Note for the 0.4 NPs, we only simulated the fraction of NPs that have more than 1 NP per sphere (see table S2 for more details).



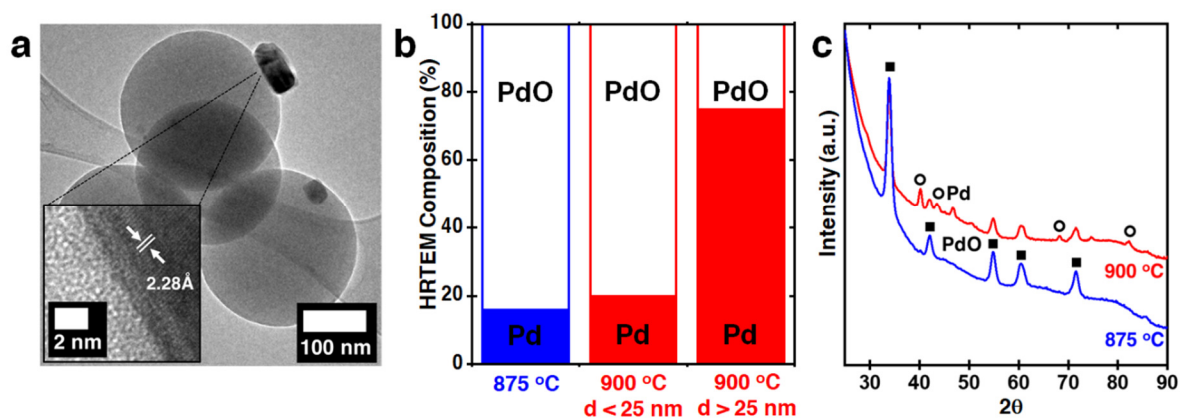
Supporting Figure S7: Analysis of low-temperature particle fusion. (a) Representative TEM image of 62-Pd/SiO₂ after aging at 800 °C for 5 h in static air. Red arrows point to the formation of NC dimers, and white arrow points to a NC trimer. (b) Distribution of particle projected areas for 62-Pd/SiO₂ as synthesized (black) and after aging at 800 °C for 5 h in static air (red). Note the formation of a bimodal PSD after aging at double the main peak area (161 nm²), indicating formation of NC dimers. Inset: posited mechanism of NP fusion due to oxidative fusion and coalescence of NCs within a critical fusion distance, first proposed by Wynblatt and Gjostein ref (1). (c) Experimental data (colored stars represent densities shown in Figures 5, 6) and simulated data (grey circles) of percentage of NCs that are fused versus NC density. Fusion percentage is calculated by taking the percentage difference in NC density between as-synthesized materials, and the NC density after aging at 800 °C. Simulations based on randomly populating spheres with NCs. *d* represents a defined parameter, representing the distance between NCs that would lead to fusion. Data best matches the *d* = 8 nm scenario, suggesting that particles will fuse if they are within 8 nm of each other.



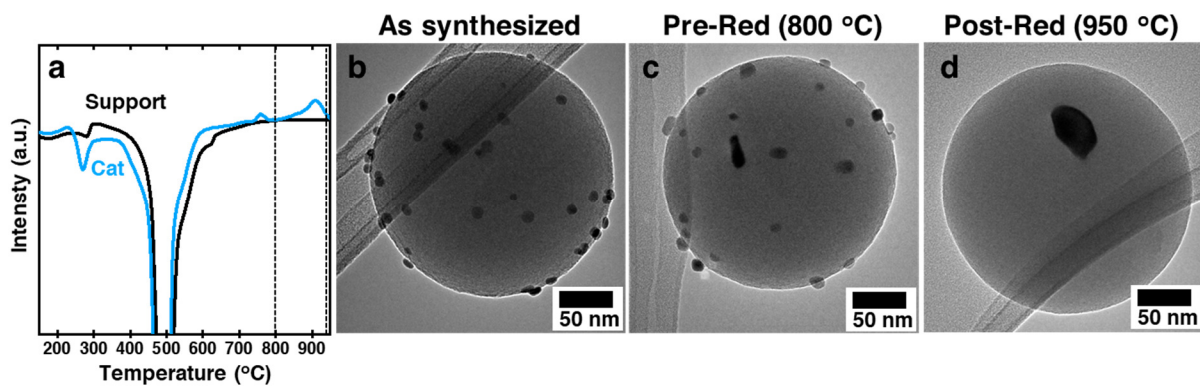
Supporting Figure S8: (a) ATR-FTIR spectra of 8.8 nm Pd/SiO₂ nanomaterial after aging treatments. *Ex-situ* attenuated total reflectance Fourier-transform infrared spectroscopy (ATR-FTIR) of aged 17-Pd/SiO₂ nanocomposites. Absorption bands between 800 cm⁻¹ and 1250 cm⁻¹ are associated with SiO₂ peaks, specifically symmetric Si-O vibration (795 cm⁻¹), asymmetric Si-OH vibration (950 cm⁻¹), and asymmetric Si-O vibration (1090 cm⁻¹). Although the Si-OH vibration vanishes upon heating to 800 °C, no further obvious change in spectrum is observed upon further heating, suggesting changed support surface chemistry does not explain the sintering processes observed at high-temperature.



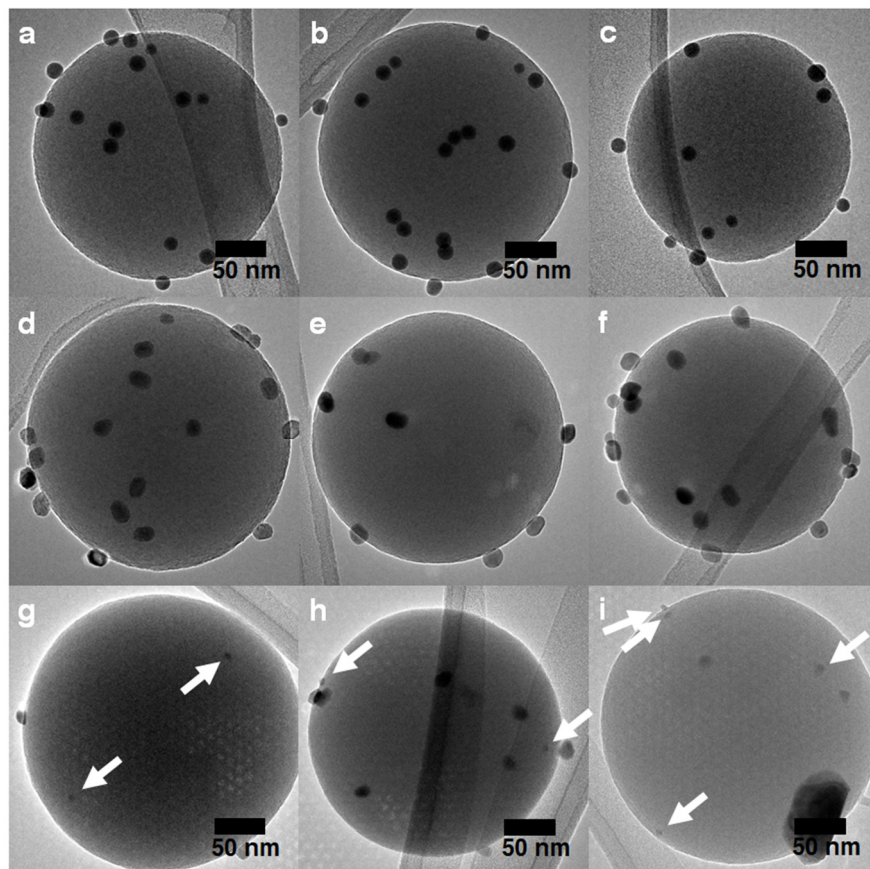
Supporting Figure S9 (a) TEM image of 8.8 nm Pd/SiO₂ nanocomposite after aging and rapid cool-down from 900 °C. Inset: Representative HR-TEM image and lattice indexing indicating metallic Pd phase. (b) Lattice imaging analysis and statistics of 50 total HRTEM images of 8.8 nm Pd/SiO₂ material after aging at 875 °C and 900 °C and rapid cool-down. (c) From the same materials, X-ray diffractograms.



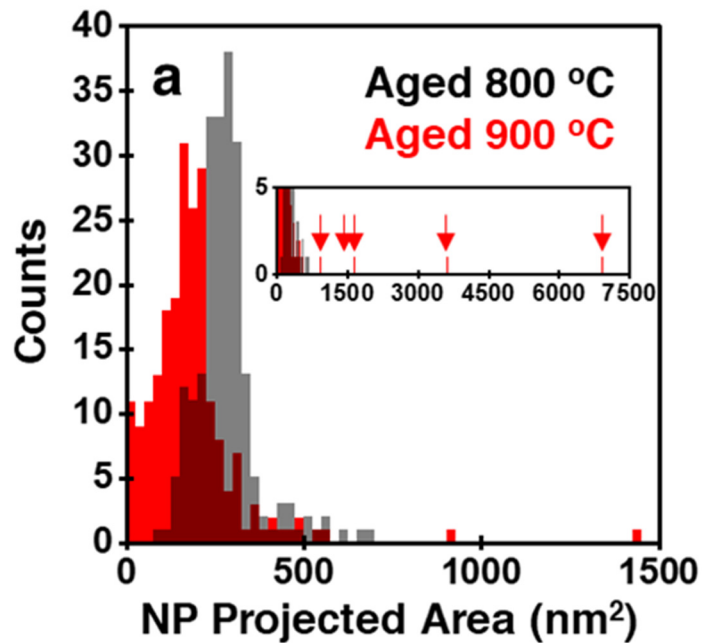
Supporting Figure S10: temperature-programmed O₂ evolution versus material stability. (a) Oxygen signal versus temperature for dried SiO₂ support and impregnated Pd/SiO₂ nanocomposite. Features at T > 700 °C correspond to PdO reduction to Pd. (b) nanocomposite as-synthesized, (c) nanocomposite recovered after 800 °C treatment and (d) after 950 °C treatment, showing how reduction leads to loss of 93% of NP surface density.



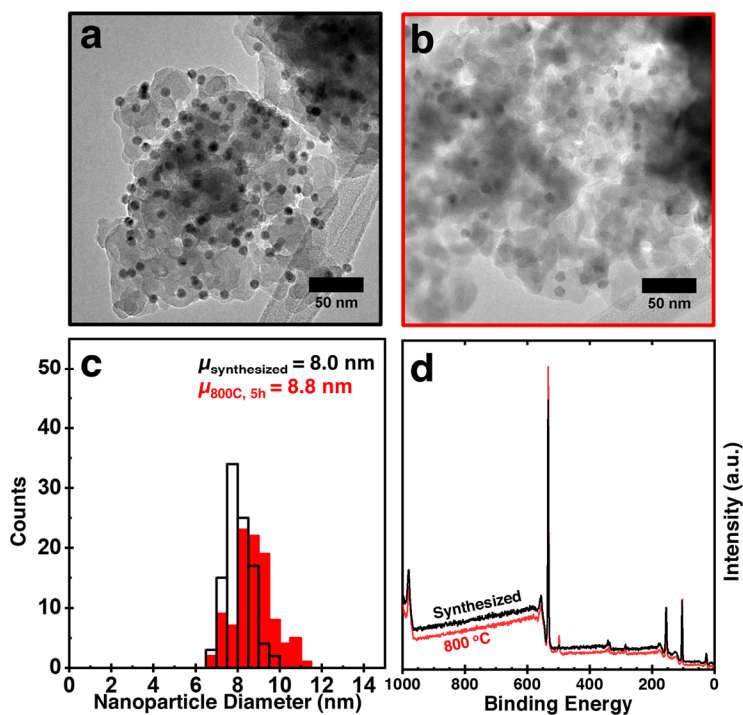
Supporting Figure S11: representative TEM images of 14.7 nm Pd/SiO₂ after various aging treatments. 14.7 nm Pd/SiO₂ (a-c) as-synthesized (d-f) 800 °C 5h static air and (g-i) 900 °C 5 h static air. Note the emergence of smaller-than-original Pd NPs after 900 °C aging treatment, as indicated by white arrows.



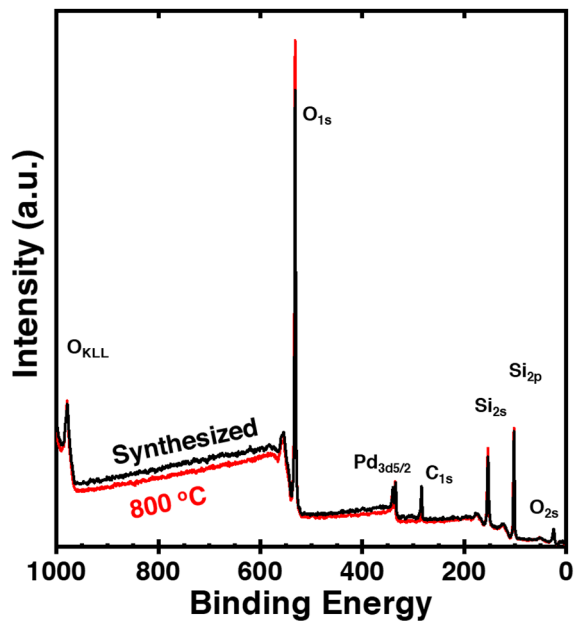
Supporting Figure S12: particle size distribution analysis reveals ostwald (atomic) ripening. Particle projected area distributions of 14.7 nm Pd/SiO₂ material after aging treatments at 800 °C or 900 °C for 5 h in static air (N = 200). Inset shows the long tail of the particle size distribution after aging at 900 °C.



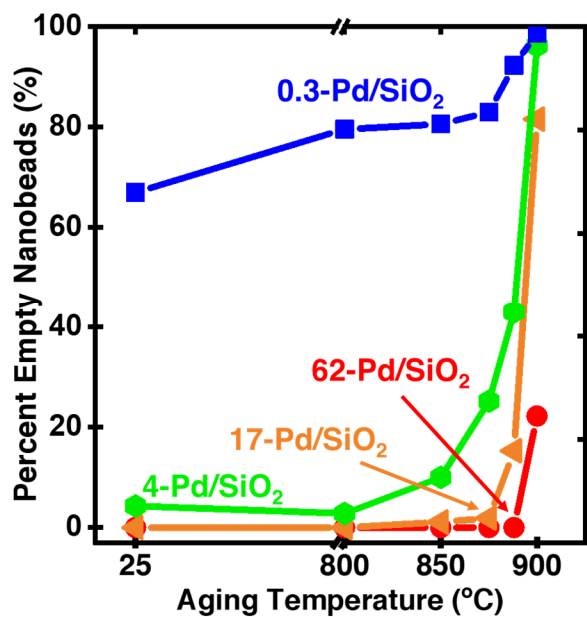
Supporting Figure S13: Thermal stability study of Pd/SiO₂ synthesized on commercial Davisil SiO₂. (a) Material as-synthesized, and (b) after 5 hrs aging at 800 °C in 4% O₂/Ar. (c) Particle size distributions before and after aging. Note that the distribution of sizes maintains a gaussian shape, without emergence of much smaller or larger particles. A slight shift in the mean value of the NP diameter is explained by oxidative expansion of the originally metallic Pd NCs (**Table S2**). (d) X-ray Photoelectron Spectroscopy measurements Davisil Pd/SiO₂ material as-synthesized (black) and after aging (red).



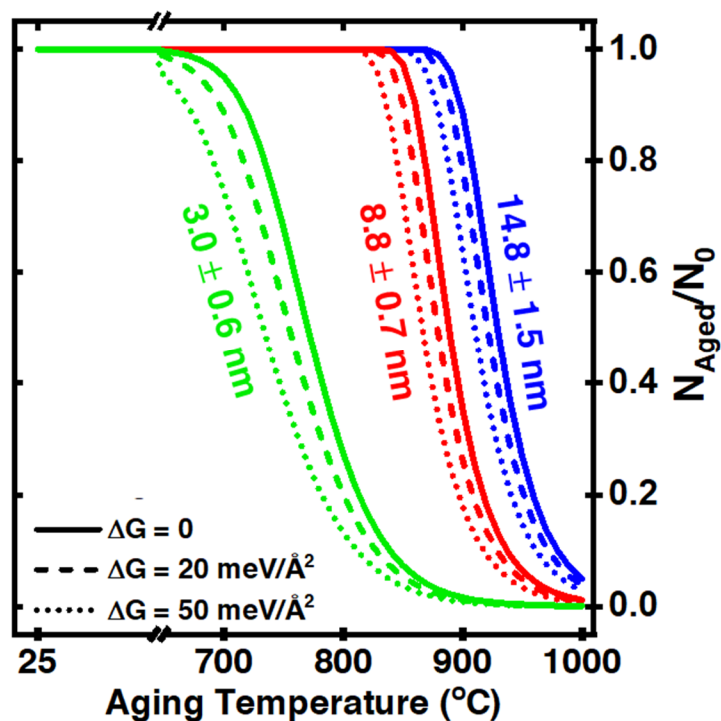
Supporting Figure S14: x-ray photoelectron spectroscopy survey scans of 62-Pd/SiO₂ nanocomposites as-synthesized (black) and after aging at 800 °C for 5 h (red). Here, we observe no signals other than those present in Pd, Si, O, and C, suggesting any surface impurities would be in very small concentrations (i.e. < 1.0 at %).



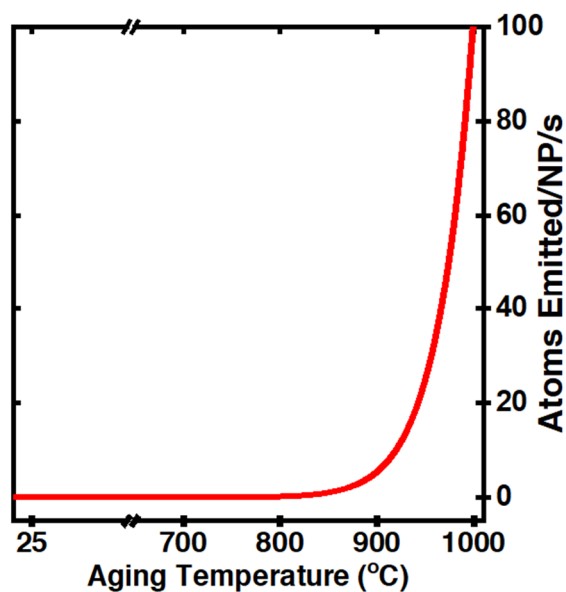
Supporting Figure S15: tracking empty SiO₂ spheres on density-controlled 8.8 nm Pd/SiO₂ samples. Percent of empty SiO₂ spheres for each of the samples shown in Figure 5 as a function of aging temperature.



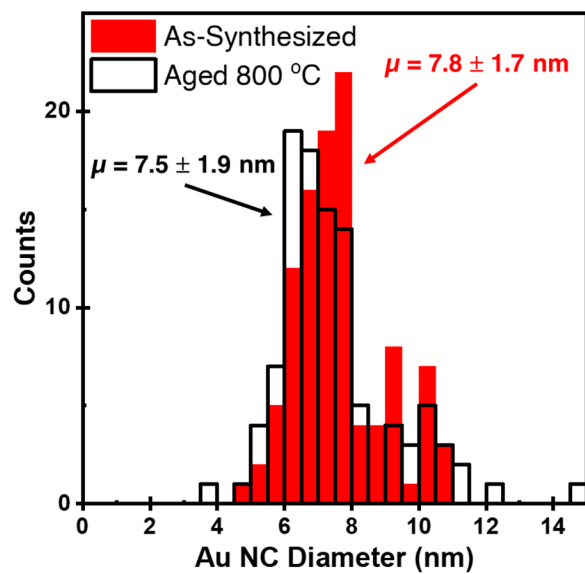
Supporting Figure S16: size-dependent vapor phase sintering simulations of metallic Pd. Simulated changes in NC density for vapor-phase metallic Pd sintering. Simulations ran to simulate 5 h aging at given temperature. Different colors represent different initial nanocrystal sizes and uniformity, based off the materials shown in Figure 1. Solid, dashed, and dotted lines represent surface energy corrections, where $\Delta G = 0$ comes from ref (2).



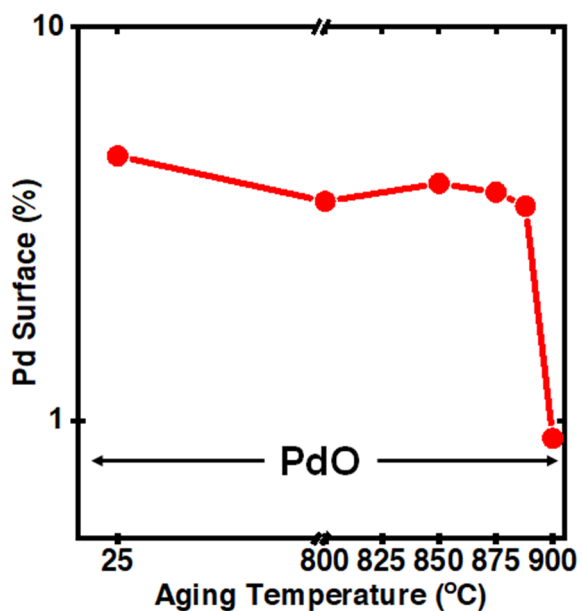
Supporting Figure S17: rate of atomic emission from surface of 8.8 nm Pd NP. Vapor-pressure taken from bulk Pd, which was consistently reported between sources refs (3, 4). From bulk vapor pressures, atoms emitted per NP per second were calculated via standard impingement (bombardment) calculations, via $Z_{\text{bombardment}} = P/(2\pi MKT)^{0.5}$, which gives atoms emitted/m²/s. To obtain emission on a per nanoparticle basis, this value was multiplied by the surface area of a hemispherical 8.8 nm NP, or 121 nm². To calculate how long it would take a NP to completely exchange all of its atoms in equilibrium, the total atomic volume of an 8.8 nm NP (~24000 atoms) is divided by 5.5 atoms/s, suggesting that a NP would emit its entire volume (in equilibrium) every 72 minutes.



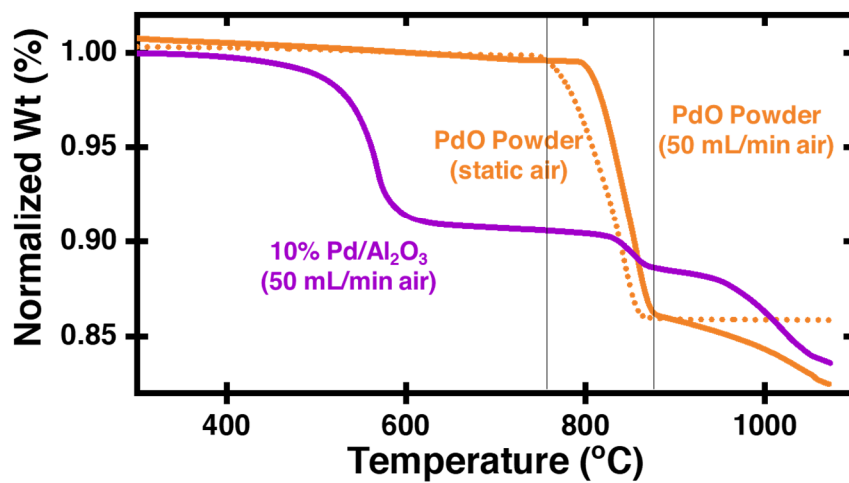
Supporting Figure S18: Particle size distributions of Au/SiO₂ material as synthesized and after aging at 800 °C for 5 h in static calcination in air.



Supporting Figure S19: x-ray photoelectron spectroscopy of 62-Pd/SiO₂ nanocomposites after aging treatments. Quantification of Pd to SiO₂ ratio for densest nanocomposite after aging treatment, corroborating stability of Pd nanocomposite until 888 °C, at which point severe reduction of exposed surface area occurs. XPS showed PdO across materials, motivating the use of rapid cool-down strategies used in Fig 3.



Supporting Figure S20: Reference thermogravimetric analyses of PdO materials. Note that loss of mass for materials in the range of 775 to 900 °C signifies a phase change from PdO to Pd.



Supporting Table S1: additional characterization of Pd/SiO₂ materials used in this work.

From Figure 2 in the main text:

Material Description	Measured Statistics (NCs/SiO₂)	Targeted Pd Loading*
3.0nm Pd/SiO₂	N/A (difficult to measure due to size)	0.1% Pd
8.8nm Pd/SiO₂	Mean: 16.8 (N = 177)	0.6% Pd
14.8nm Pd/SiO₂	Mean: 3.6 (N = 163)	1.6% Pd

*This number is calculated via dividing the mass of Pd, as calculated via TGA of the Pd NC solution, by the mass of SiO₂.

From Figure 5 in the main text:

Material Description	Measured Statistics	u_{NND}	Normalized Diffusion time
62-Pd/SiO₂	Mean: 61.9 (N = 170)	26 nm	1
17-Pd/SiO₂	Mean: 16.8 (N = 177)	51 nm	3.8
4-Pd/SiO₂	Mean: 3.6 (N = 163)	114 nm	19.2
0.5-Pd/SiO₂	Mean: 0.42 (N = 224)	173 nm*	> 44.3*

*Assuming diffusional processes scale $\sim x^{0.5}$. These calculations don't include the fraction of SiO₂ which have 1 NP. These would likely lead to larger NNDs due to traversing across an entire sphere, which may drastically influence the time of diffusion between NPs.

Supporting Table S2: Calculations for size change for NP oxidation from Pd to PdO.

Material	Pd	PdO
lattice parameters	a = 0.38898 nm	a = 0.302 nm, c = 0.531 nm
unit cell volume	$a^3 = 0.058855 \text{ nm}^3$	$a^2c = 0.048429 \text{ nm}^3$
Pd atoms/unit cell	4 atoms	2 atoms
nm³/Pd atom	0.014714 nm ³	0.024215 nm ³
NP diameter	3.0 nm 8.8 nm 14.8 nm	3.5 nm 10.4 nm 17.5 nm

Supporting Table S3: Surface energies for Pd and Au and parameters of temperature T [K]

dependent vapor pressure for Pd [atm]: $\log_{10} p = A + \frac{B}{T} + C \log_{10} T$ and Au (5) [bar]: $\log_{10} p =$

$A - \left(\frac{B}{T+C}\right)$ as used in the Ostwald ripening mean-field model.

Material	Pd	Au
Surface energy	$\gamma = 108.80 \text{ meV/\AA}^2$	$\gamma = 83.21 \text{ meV/\AA}^2$
Parameters of temperature T dependent vapor pressure	A=9.502 B=-19813 C=-0.9258	A=5.46951 B=17292.476 C=-70.978

References

1. P. Wynblatt, N. A. Gjostein, Particle growth in model supported catalysts-i. theory. *Acta Metall.* **24**, 1165–1174 (1976).
2. W. R. Tyson, SURFACE FREE ENERGIES OF SOLID METALS ESTIMATION FROM LIQUID SURFACE TENSION MEASUREMENTS. *Surf. Sci.* **62**, 267–276 (1977).
3. H. R F, W. R F, The vapor pressure of palladium. *J. Phys. Chem.* **66A**, 177–178 (1962).
4. C. B. Alcock, V. P. Itkin, M. K. Horrigan, Vapour Pressure Equations for the Metallic Elements: 298–2500K. *Can. Metall. Q.*, 309–313 (2013).
5. D. R. Stull, Vapor Pressure of Pure Substances ORGANIC COMPOUNDS. *Ind. Eng. Chem.* **39**, 518–540 (1947).